VALIDATION OF NUMERICAL PROCEDURE FOR ASSESSMENT OF CENTRIFUGAL PUMP CAVITATION EROSION

by

Serguei F. Timouchev
Professor
Moscow Aviation Institute
Moscow, Russia

Sergey S. Panaiotti
Professor
Moscow Bauman State Technical University
Moscow, Russia

Vladimir A. Knyazev
Senior Staff Scientist
Russian Research Center, Kurchatov Institute
Moscow, Russia

and

Vladimir A. Soldatov
Senior Staff Scientist
Russian Research Center, Kurchatov Institute
Moscow, Russia

Serguei Timouchev is Professor of Turbomachinery, Head of the Laboratory of Numerical Modeling of the Scientific Research Centre of New Technologies in MAI, and Director General of InteRe Ltd., in Moscow, Russia. He began his career in 1980, working for the Buran space program in the NPO Energomash. Dr. Timouchev worked within the Moscow Aviation Institute for the Arianne-Vulcain project; has made experimental and computational studies in the field of pressure pulsation and vibration of centrifugal turbopump units of liquid rocket engines; proposed the original method for numerical modeling of pressure pulsation in centrifugal machines; worked on the computational prediction of pressure pulsation in centrifugal pumps and ventilators and reduction of vibration and noise; and worked for the EU scientific project NORMA on noise and vibration reduction in high-speed ships.

Dr. Timouchev graduated from Moscow Aviation Institute in 1978, and received a Russian Doctor of Technical Science degree in 1996.

Sergey S. Panaiotti is Professor in the Department of Hydraulic Machines in the Moscow Bauman State Technical University, in Moscow, Russia. He began his career as a post-graduate student in the Department of Hydraulic Machines, then Senior Lecturer (Kaluga Branch), and Head of the Department of Mechanical Engineering. Dr. Panaiotti has professional experience as a lecturer and tutor in the field of fluid mechanics, centrifugal and axial flow pumps, hydraulic turbines, dynamic pump systems and equipment, and CAD of dynamic pumps. His research interests comprise applied hydrodynamics, centrifugal, axial, and special pumps with high suction capability. He participates in contract work with industrial enterprises and research institutes primarily in the design of condensate, boiler feed, and rocket engine pumps.

Dr. Panaiotti graduated from Krasnodar Food Industry Institute in 1961, and has a Russian Doctor of Technical Science degree. He also is translator of the Russian edition of the Transactions of ASME.

Vladimir A. Knyazev is Senior Staff Scientist with the Russian Research Center, Kurchatov Institute, in Moscow, Russia. He participated in the design of nuclear reactors of different types, and was the project leader of gas-cooled fast breeder BGR-300. He specialized in the field of subcooled liquid boiling, two-phase hydrodynamics, and diffusion kinetics. Mr. Knyazev studied surface boiling from the activation point up to the developed stage and found theoretically and experimentally the zone of intensive erosion of surface under subcooled liquid boiling. Currently he works on the problem of volume boiling in the emergency process of decompression. He intensively worked in the theory of hydromechanics for a better explanation of turbulent flows. It was proved that the classical Navier-Stokes hydromechanics based on the pseudosolidification hypothesis does not include transition to turbulence. He proposed a hydromechanics on the basis of no decrease of entropy without using the pseudosolidification hypothesis. This gives the possibility of direct turbulent flow calculation without additional closure equations.

Mr. Knyazev graduated from Moscow Aviation Institute in 1962.

ABSTRACT

This paper presents validation of a novel method for assessment of the centrifugal pump cavitation erosion with two configurations of a model feed centrifugal pump:

- With thru shaft, and
- Cantilever impeller.

The method combines 3D unsteady flow computational fluid dynamics (CFD) modeling and numerical analysis of cavitation bubbles behavior. The method considers evolution of the bubble in nonuniform 3D flow from initial onset conditions until the disruption moment with determination of the erosion jet power impact.

INTRODUCTION

The mechanism of cavitation erosion has been studied for more than a hundred years, but until now there has been no general theory of cavitation erosion damage to analytically calculate cavitation erosion rate in impellers of centrifugal pumps or to evaluate erosion intensity at the pump design stage. Meanwhile, the task of increasing a pump's lifetime up to 40,000 hours becomes an actual one. In solving this task, new impeller blade geometries and semi-empirical methods are used for prediction of cavitation erosion damage (Gopalakrishnan, 1985; Visser, et al., 1999). It appears that the common methods of providing required net positive suction head (NPSH) level are not satisfactory for the development of new high life-cycle pump impellers as unsteady inlet flow characteristics influence cavitation erosion intensity as well. The novel method consisting of numerical unsteady flow modeling and direct modeling of the cavitation bubble collapse process is proposed to solve both issues—flow unsteadiness effect and evaluation of wall stresses (Knyazev, et al., 2007). Nonuniform pressure-velocity field is obtained by CFD unsteady 3D turbulent flow analysis based on an established fact that the major effect of erosion damage is observed in the mode of operation between the incipient cavitation mode and the "NPSH-3%" mode, i.e., in the mode of operation where the vapor volume effect on flow characteristics can be neglected. The proposed numerical procedure is validated with the experimental data of two alternative model pump designs (Panaiotti, et al., 2007). The designs represent the first stage of a multistage centrifugal feed pump. Usually such a pump has a long through shaft of large diameter with two tip shaft seals, oil lubrication bearings installed beyond the pump casing, and a lateral fluid inlet to the first stage. The through shaft increases fluid velocity at the impeller inlet reducing cavitation quality, and strengthens cavitation erosion of the pump first stage. This design concept is conventional. During activity under the contract a new design was developed. It has a first stage cantilevered impeller and axial fluid inlet. The pump shaft rotates in two hydrodynamic bearings fed by the pumping fluid. The first bearing bushing is located in the vane stator disk bore, and the second, before the unique tip shaft seal at the pump drive side. Cantilever centrifugal impeller installation of the first stage decreases input diameter and relative flow velocity at the blade input. Its eye diameter decreases significantly and the relative velocity of the flow at leading edges of impeller blades drops. This makes the erosion rate decrease by several times. Comparative experimental study of these alternative designs produces a basis of the numerical method validation.

TEST RIG AND PUMP TEST STAGE

The cavitation erosion study was performed using the test rig shown in Figure 1. The supplying tank (1) of the pumping installation is filled with water from the water supply. The pressure at the experimental pump inlet is measured by the absolute pressure gauge (11) or standard spring manometer (10). Manometer (11) is connected to the pressure taps through the separating vessel. For reverse flows at the impeller inlet not to influence the measured inlet pressure, a solid cascade (16) of thin radial sheets is installed in the suction duct. A wide range of pressure at the pump inlet can be set by changing the pressure in the supply tank. To do this, a piston (15) and water-packed ring-type vacuum pumps (14) are connected to the tank. The fluid temperature is measured by a thermometer (3) and can be controlled by the water cooler (20). The fluid level in the supply tank is read from the level meter; the fluid-free surface pressure is read from the vacuum-pressure gauge. The flow meter (12), equipped with a mercury differential manometer, measures the pump flow rate. The slide-valve (8) controls the pump flow rate. To ensure increased pressure at the flow meter device section thus eliminating cavitation in it, the additional slide-valve (19) is installed after the flow meter. The pump head rise is calculated by using the readings of the pressure gauges (9, 10, or 11), while velocity heads are calculated. The pump NPSH is determined by using the pressure gauge (11) readings, calculated velocity head, and vapor pressure. The last is determined by water temperature at the pump inlet. The thermometer (3) measures this temperature. The pump test is driven by a direct current (DC) electric torque meter (5) with a weight-meter (using its readings, one determines the pump consumed power). The motor power is 70 kW; maximum rotor rotational speed is 4000 rpm. The pump rotor rotational speed is measured by a tachometer, which consists of the induction probe (6) and speed meter (7). Pulsation pressure sensors are mounted in the input and output pipe of the test pump; vibration acceleration sensors are mounted on the horizontal and vertical planes in the pump housing. For these studies the test pump was modernized as shown in Figure 2. The test pump flow part has a transparent reducer (6) and transparent cover (5) made from Plexiglas®. Impeller #1 with through shaft (upper part) and cantilever impeller #2 (lower part) have removable transparent front disks. Transparent parts of the test rig allow observation of fluid flow inside the impeller for the various cavitation modes. It is possible to determine the reverse flow onset at the pump inlet with flexible fibers.

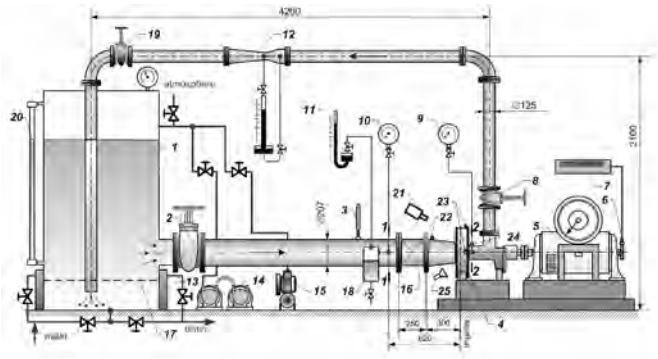

1 - Tank 1.4 m^3; 2 - Valve; 3 - Thermometer with Scale Factor 0.1°C; 4 - Test Pump; 5 - Torque Meter; 6 - Induction Probe; 7 - Speed Meter; 8 - Control Valve; 9 - Discharge Manometer; 10 - Suction Manometer; 11 - Mercury Absolute Pressure Gauge; 12 - Flow Meter; 13 - Water Cooler; 14 - Vacuum Pumps; 15 - Compressor; 16 - Radial Sheets; 17 - Screen; 18 - Separating Vessel; 19 - Flow Meter Control Valve; 20 - Level Meter; 21 - Digital Camera; 22 - Input Pressure Pulsation Sensor; 23 - Vibration Acceleration Sensors; 24 - Output Pressure Pulsation Sensor; 25 - Stroboscope.

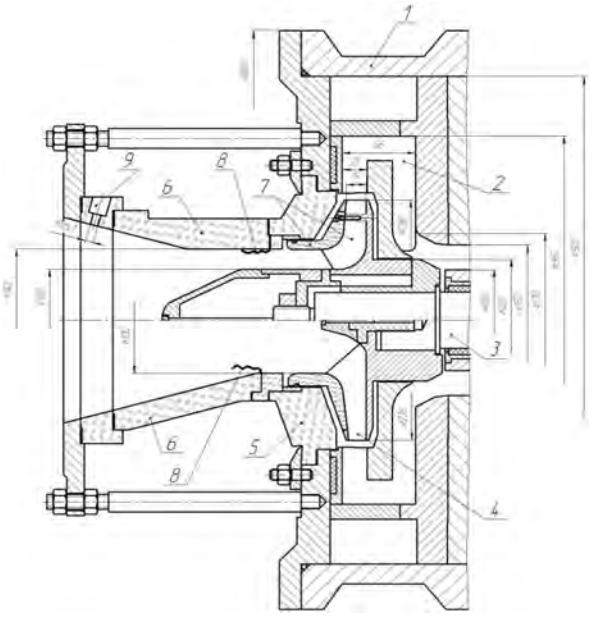

Figure 2. Test Configurations #1 (Above Axis) and #2 (Below Axis) (Dimensions in mm): 1 - Pump Housing; 2 - Vaned Diffuser; 3 - Shaft; 4 - Impeller #2; 5 - Transparent Cover; 6 - Reducer; 7 -Impeller #1; 8 - Flexible Fiber; 9 - Hole for the Pressure Pulsation Sensor.

IMPELLER DESIGNS

Two impeller designs were developed in the course of a research grant. The cavitation erosion rate is proportional to the sixth degree of the circumferential velocity at the impeller eye diameter. Therefore, with reduction of this diameter the cavitation erosion rate will drop for the cantilever impeller design.

Centrifugal impeller #1 is designed for a pump inlet with through shaft. In that case the hub extended upstream simulates the thru shaft. The centrifugal impeller #2 was designed like the cantilever one. Both centrifugal impellers are contoured by a conformal mapping method. The impeller blades have cylindrical form at the exit and inlet spatial shape providing small positive angles of attack at the design capacity.

For both the model configuration #1 with thru shaft and the model configuration #2 with cantilever impeller the design parameters were:

- flow rate Q = 0.019m^3/s, head H = 69 m, rotation speed n = 3000 rpm , specific speed (in Russian notation, see "NOMENCLATURE") n_s = 105 or N_s (US) = 1486, head break cavitation specific speed $C_{III} \approx 1300$.

Impellers are designed with the plane hydrodynamic blade cascade theory. Cavitation calculation is done under the theory of free stream frictionless flow in the finite thickness blade cascade. The blade leading edge camberline angle at the shroud of impeller #1 is 17.4 degrees and 31.6 degrees at the hub. The outlet angles of both impellers are 22 degrees. At the design point the incidence angle at the shroud is equal to 1.6 degrees. The same angles for impeller #2 are 24.6 degrees, 45.2 degrees, and 1.3 degrees, respectively. Other dimensions are shown in Figure 2. The vaned diffuser is designed with the one-dimensional theory by using empirical data. A photo of impeller #1 is shown in Figure 3. Impeller #2 is characterized with a hub of small diameter, 26 mm. Having the same calculated head break suction specific speed C_{III} = 1300 as impeller #1, this impeller has a much smaller eye diameter 100 mm, than impeller #1, which has an eye diameter of 142 mm. This ensures that circumferential velocity at eye diameter drops by 1.4 times. The latter leads to decrease cavitation erosion rate for impeller #2 approximately by $1.4^6 = 7.5$ times compared to impeller #1 under the same operation conditions.

Figure 3. Impeller #1.

Photo of impeller #2 is shown in Figure 4. Both impellers have a dismountable cover disc made of Plexiglas®, which allows visual observation and photography of incipience and development of cavitation in flow passage of the impeller. It also simplifies the process of blade passages coating with varnish and examination of varnish destruction patterns. Test impellers #1 and #2 have seven working blades and the vane diffuser has nine channels. In CFD calculations, the vaned diffuser is simplified with a vaneless diffuser.

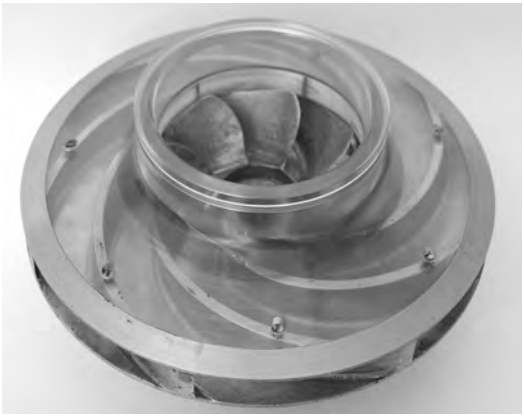

Figure 4. Impeller #2.

The test stage vaned diffuser (Figure 2, position 2) has an outer diameter of 360 mm and width of 68 mm. An overall view of the vaned diffuser is shown in Figure 5. The flow part consists of nine continuous channels, including spiral ducts (1), diffusers (2), transferring ducts (3), and return ducts (4). Spiral ducts gather liquid and decrease velocity momentum after the impeller. Diffusers transform velocity head into pressure energy. In a multistage pump the transferring ducts convey the liquid from diffusers to return ducts supplying liquid to a next pump stage. In the test pump liquid comes from return ducts into the annular chamber where the gauge section for pump outlet pressure is located.

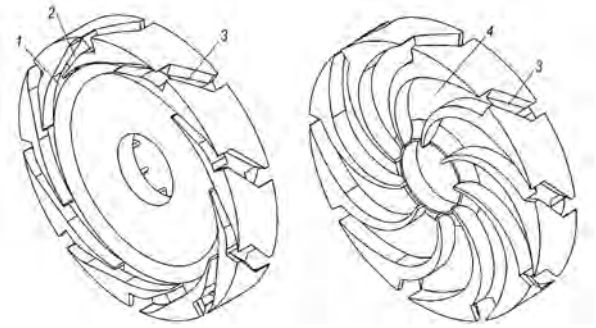

Figure 5. Vaned Diffuser: 1 - Spiral Duct; 2 - Diffuser Duct; 3 - Transferring Duct; 4 - Return Duct.

CAVITATION EROSION ONSET EVALUATION

Despite the great number of papers on the cavitation erosion problem, prediction of cavitation erosion rate for centrifugal pump blades is rather uncertain. There are methods (Gülich, 1997; Sloteman, et al., 2004) linking cavitation erosion rate with the cavity length using semi-empirical formulas.

Experiments include visual observations of cavities with the use of a stroboscope, cavities photography with small exposure time, and cavity length measurement. Cavitation inception inside the impeller is accompanied with hydrodynamic noise, pressure pulsations, and pump housing vibration. According to Gülich (1992, 1997), Gülich and Pace (1986), and many others, there is a connection between pump housing vibration and cavitation erosion intensity—the more vibration, the more erosion intensity. The pump housing vibration acceleration and pressure pulsations at pump suction and discharge are registered during tests. According to Gülich and Pace (1986), cavitation erosion rate is proportionate to effective vibration acceleration of pump housing. Estimation and registration of the vibration acceleration of the pump housing are performed in the vertical and horizontal direction. The scheme of sensors installation is shown in Figure 1. Piezoelectric accelerometers were selected. Sensors that use integrated circuit piezoelectric (ICP) technology are preferred since they produce minimal measurement error. Pressure pulsation sensors are installed at pump inlet and outlet (Figure 1). Sensor diaphragms are flush-mounted with inner walls of the housing. Highly sensitive piezoelectric pressure sensors at inlet and at outlet were used for the estimation and registration of the pressure pulsation in the suction and at the discharge of the pump. In this paper only housing vibration data are outlined. For the vibration parameter the vertical (av) and horizontal (ah) housing vibration acceleration root-mean-square (RMS) value, in 5…46 kHz frequency range were chosen.

The root-mean-square value of vibration is calculated with averaging time T_a = 5s. Root-mean-square value is calculated according to Equation (1):

$$a'_{RMS} = \sqrt{\sum_{i=1}^{n} x_i^2 / n} \quad \textbf{(1)}$$

where x_i = current value of the parameter, n = 500,000—amount of the counting for averaging time of T_a = 5s. In order to exclude the background component of vibration acceleration, it is corrected by the formula:

$$a_{RMS} = \sqrt{a'^2_{RMS} - a^2_{RMS\,0}} \quad \textbf{(2)}$$

where $a_{RMS\,0}$ = the root-mean-square value of the vibration acceleration in the noncavitational operation pump mode (with NPSH more than 11 m). Vibration level in decibel (dB) scale is calculated with the formula:

$$L_a = 20\log(a_{RMS} / a_r) \quad \textbf{(3)}$$

where $a_r = 3\cdot10^{-4}$ m/s^2—reference value.

Easily-destructible varnish coatings are used to rapidly determine the places of cavitation erosion damage of impeller material (Figure 6). If there are no places of varnish damage during the prolonged cavitation experiment, then one can suppose that there is no cavitation erosion damage of impeller material. Black heat-resistant organosilicon varnish was used. The transparent impeller cover disc was at first dismounted. Then, the impeller was painted with a brush and dried in the drying chamber at 50°C for one hour. Next, the impeller is assembled and installed into the test pump. Experiment duration is set to 120 minutes for all experiments with the varnish coating destruction check. Varnish coating is destroyed up to impeller's metal.

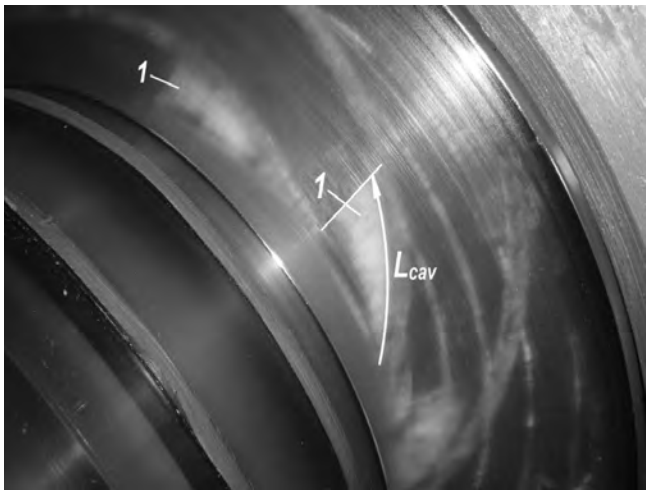

Figure 6. Cavity Photo: 1 - Cavity Closure Region.

Performance Characteristics

Performance tests of the two experimental pump configurations are conducted at constant rotor speed of n = 3000 rpm. To totally avoid cavitation the overpressure in the supply tank is increased making NPSH Δh = 20…25 m.

Figure 7 shows the H(Q) performance of the experimental pump configuration with centrifugal impeller #1 (the variant with thru shaft). The H(Q) curve from shutoff (zero flow) up to 0.03 m^3/s is almost horizontal. The best efficiency point Q_{BEP} = 0.049 m^3/s corresponds to the design point. The maximum efficiency is η_{MAX} = 79 percent. The specific speed is n_s = 106 (N_s = 1500). The stage head rise coefficient, characterizing the impeller radial size is $H = gH/U_2^2 = 0.46$. Observation of flexible fiber deflection shows (Figure 2, position 8) that the reverse flow at the impeller #1 inlet appears at critical flow rate of Q_{cr} = 0.0299 m^3/s = 0.61 Q_{BEP}. Because of this, at Q > 0.0299 m^3/s the pump can operate without low-frequency pulsations of pressure and flow rate. Moreover, Figure 7 presents the $\Delta h_{III} = f(Q)$ curve. Figure 8 shows the performance characteristics of impeller #2. The optimum operating conditions are: Q_{BEP} = 0.049 m^3/c, H_{BEP} = 67 m, η_{MAX} = 82 percent.

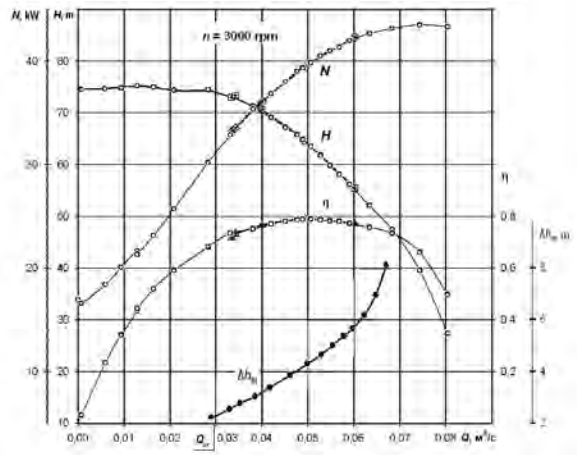

Figure 7. Performance Characteristics of the Configuration with Impeller #1.

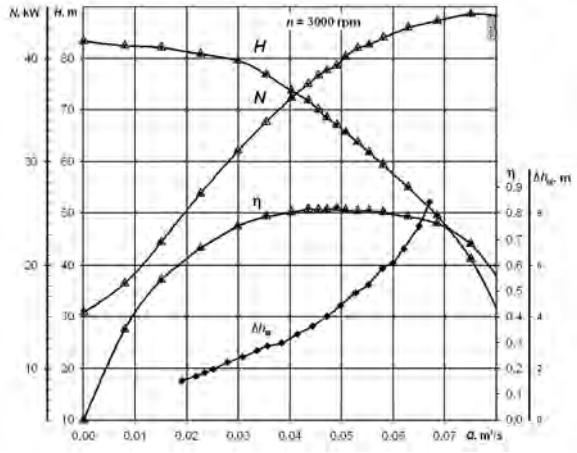

Figure 8. Performance Characteristics of the Configuration with Impeller #2.

NPSH Performance

During the tests of NPSH performance H(Δh), N(Δh), the measurements of housing vibration L_a = f(Δh) and cavity length are also completed.

Figure 9 presents the NPSH performance H(Δh), N(Δh) at the optimum operating condition Q = 0.049 m^3s, n = 3000 rpm for the configuration with impeller #1. Head rise started to reduce at NPSH Δh_I = 5.4 m, which corresponds to C_I = 1054. When the head rise is reduced by 3 percent, the NPSH $\Delta h_{3\%}$ = 4.5 m ($C_{3\%}$ = 1190). The full head breakdown condition is Δh_{III} = 4.35 m (C_{III} = 1240).

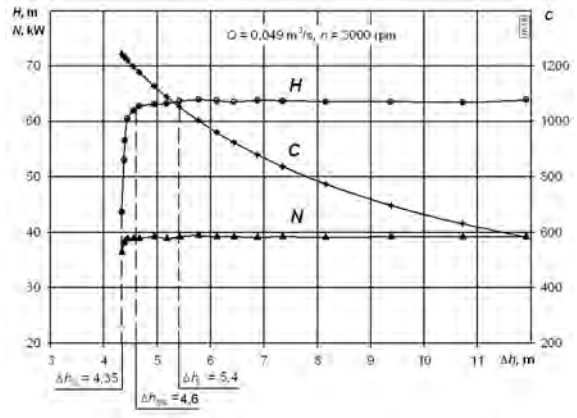

Figure 9. NPSH Performance of the Configuration with Impeller #1.

The cavity lengths were measured at different NPSH levels in impellers #1 and #2 (Figure 10). The test rig had limitations for full visual access; the cavity lengths of 20 mm or above could be measured. Furthermore, this figure shows the H = f (Δh) curves as well. The cavity lengths in different channels of impeller #1 differ from each other to some extent. The cavity length was measured in the channels between the fifth and seventh blades and the cavity length in Figure 10 is an average length. As the NPSH reduces, the cavity length increases. At Δh ≈ $\Delta h_{3\%}$ the cavity length is nearly the same as the blade pitch at impeller tip inlet 64 mm. Further NPSH decreasing causes the cavity to grow rapidly; the cavity collapse area reaches the impeller outlet diameter.

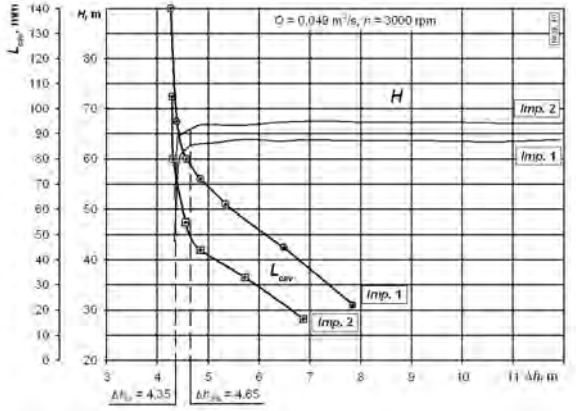

Figure 10. The Dependence of Cavity Length upon NPSH for Impellers #1, 2.

The corresponding vibration-cavitation performance L_a (Δh) is shown in Figure 11. Effective vibration accelerations of the stage casing with impeller #1 started to grow at Δh = 10.7 m. When the NPSH reduces, vibration accelerations increase slowly in the NPSH range of 10.7 m < Δh < 8.15 m. Then at Δh < 8.15 m, accelerations increase rapidly. Taking that into account, it can be inferred that the cavitation processes in impeller #1 appear at Δh = 10.7 m (C = 630). Therefore, to totally avoid cavitation erosion with impeller #1, a suction head (NPSH) Δh > 11 m is needed.

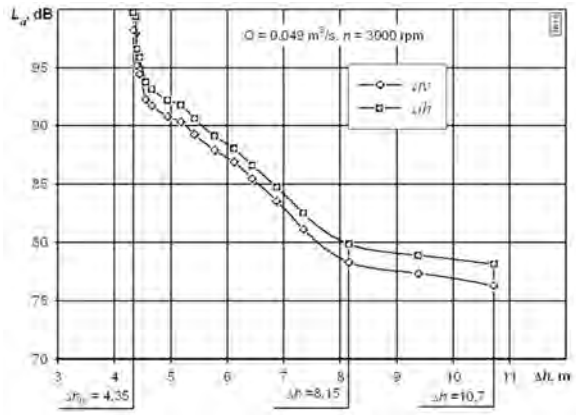

Figure 11. Vibration-Cavitation Performance of the Configuration with Impeller #1: av, ah - Vertical and Horizontal Vibration Levels, Respectively.

To observe varnish coating damages the NPSH range of Δh = 4.85…7.8 m was chosen. Damages were studied at right and left limits of this range. The right limit Δh = 7.8m (C = 800) corresponds to average suction ability of a pump, while the left limit is Δh = 4.85 m (C = 1130 [N_{SS} =10,385]), i.e., near $\Delta h_{3\%}$. For configurations #1 and #2 identical boundaries of NPSH were taken.

Figure 12 shows varnish damage at Δh = 7.8 m. Damages take place only near inlet zones of impeller blades at visible sides (suction sides)

of blades. After removing the shroud disk, no damages on invisible sides (pressure sides) and in blade channels were determined. Also noted were some asymmetry of damage zones. The last fact as well as difference in cavity lengths mentioned above can be caused by unavoidable impeller fabrication inaccuracies.

Figure 12. Varnish Damages in Impeller #1 at Q = 0.049 m³/s, N = 3000 RPM, Δh = 7.8 m.

The NPSH performance of the configuration with impeller #2 is shown in Figure 13. Head rise started to drop at Δh_I = 4.85 m (C_I = 1140 [N_{SS} = 10477]); when the head rise dropped by 3 percent, the NPSH was $\Delta h_{3\%}$ = 4.65 m ($C_{3\%}$ = 1180 [N_{SS} = 10,844]). The cavitation head breakdown occurred at Δh_{III} = 4.35 m (C_{III} =1240 [N_{SS} = 11,396]). At certain NPSH, the cavities appear on the blade leading edges. With NPSH reduction, the cavity length increases. Generally the cavitation development scheme in impeller #2 is similar to that in impeller #1.

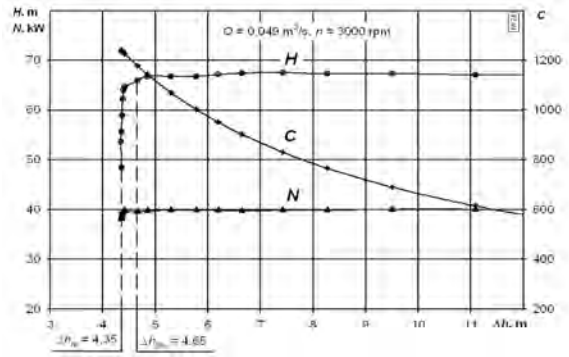

Figure 13. NPSH Performance of the Configuration with Impeller #2.

Vibration-cavitation performance of the stage with impeller #2 is shown in Figure 14. Effective vibration acceleration started to grow at Δh = 11.1 m. Rapid growth was observed at Δh = 7.45 m, and at Δh = 4.4 m it reaches its maximum.

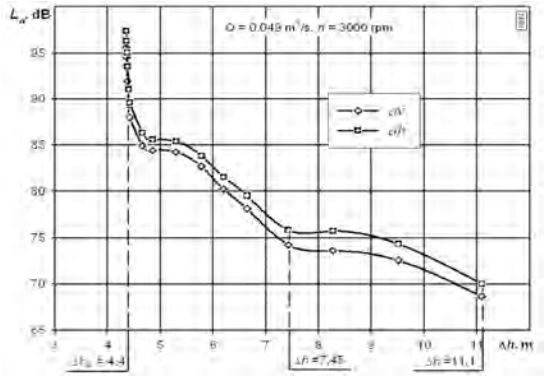

Figure 14. Vibration-Cavitation Performance of the Configuration with Impeller #2: av, ah - Vertical and Horizontal Vibration Levels, Respectively.

Impeller #2 coated with varnish was run for 120 min at Q = 0.049 m³/s, n = 3000 rpm, and Δh = 7.8 m (C = 800), that corresponds to the right limit of the NPSH range. There were no varnish damages at blade leading edges, at both blade sides, on impeller hub/shroud, or other sections of impeller ducts (Figure 15). There were varnish chips on leading edges of two blades. At the left limit of the NPSH range (Δh = 4.85 m, C = 1140), varnish was damaged at the blade suction side.

Figure 15. Centrifugal Impeller #2 after Tests at Q = 0.049 m³/s, N = 3000 RPM, Δh = 7.8 m.

NUMERICAL PROCEDURE VALIDATION

The 3D numerical procedure is based on a nonstaggered Cartesian grid with adaptive local refinement and a subgrid geometry resolution method for description of curvilinear complex boundaries. Unsteady Navier-Stokes equations are solved by applying a standard k-ε turbulence model. Computational domain consists of three subdomains—inlet, rotor, and vaneless diffuser connected by "sliding-grid" interfaces. The computational procedure (Panaiotti, et al., 2007) provides flow parameters for estimating the main energetic parameters of two impeller designs and validation of the code with experimental data.

Computational tests of impeller performance characteristics are completed on the axisymmetric adapted grid with the inlet boundary condition where volumetric flow rate is defined by the normal to boundary velocity component. For estimation of impeller cavitation behavior and erosion intensity, computational tests are made on the initial grid that has a non-uniform distribution in relation to axis of rotation. This is made for providing a denser grid at the impeller inlet. The number of computed grid cells is around 200,000.

In the inlet boundary condition the total pressure is 80334 Pa, which corresponds to an NPSH of 7.74 m under which there is an erosion damage of varnish coating for impeller #1. For the outlet boundary condition, the volumetric flow rate is defined by the normal to boundary velocity component. The presence of cavitation cavity is not accounted for in computations. Operation pump parameters are equal to experimental rotation speeds of 3000 rpm and volumetric flow rate 0.049 m³/s. A description of the computational method is outlined in previous publications (Knyazev, et al., 2007; Panaiotti, et al., 2007).

Computational domains for two impeller designs are presented in Figures 16 and 17. These figures represent a virtual link of three subdomains by sliding surfaces at the impeller inlet and outlet. These sliding interfaces serve as control surfaces and estimation of the impeller characteristics as well. In the impeller #1 design, a hub developed upstream presents the thru shaft. The part of the hub locates in the inlet motionless subdomain. The rotation of this part is accounted for by a wall velocity-swirl boundary condition.

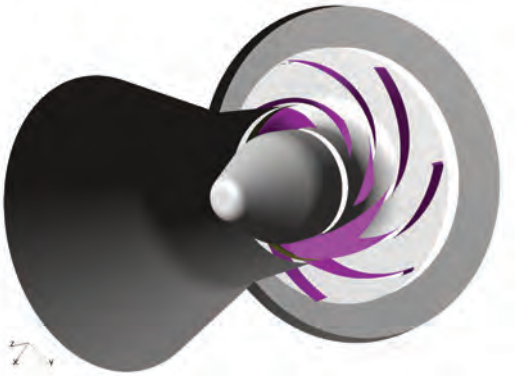

Figure 16. Impeller #1 Model with thru Shaft Simulation.

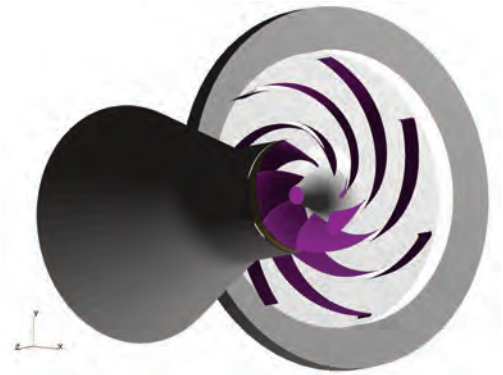

Figure 17. Model with Cantilever Impeller #2.

EVALUATION OF IMPELLER PERFORMANCE PARAMETERS

Iterative procedure goes up to convergence to a "steady" periodical solution with a time step 10^{-4} s. Resulting impeller flow characteristic parameters can be determined by time- and flow-averaging of unsteady computational flow data. The convergence is controlled by the effective head value level between inlet and outlet rotor sliding surfaces.

For definition of the impeller head and hydraulic efficiency, on each tenth iteration flow- and area-averaged total pressures p_{01}, p_{02}, meridian c_{1m}, c_{2m}, and tangential c_{1u}, c_{2u} absolute velocity components, and circumferential impeller velocities u_1 и u_2 are fixed on the rotor inlet and outlet sliding. In this way, for example, averaged total pressure is obtained by:

$$p_0 = \frac{1}{N}\sum_n \frac{1}{Q}\sum_i (\tilde{p}_{0_{n,i}} \cdot \tilde{c}_{m_{n,i}} \cdot ds_i) \qquad (4)$$

where:

N = Number of time levels
Q = Volumetric flow
n = Time step index
i = Computational cell index
$\tilde{P}0_{ni,}$ = Total pressure value in i-cell for n-time step
$\tilde{c}_{m_{ni,}}$ = Meridian velocity component in i-cell for n-time step
ds_i = Cross section i-cell area

Other parameters are obtained in a similar manner. Leakage losses in this computation are not accounted for. Effective impeller head is given by:

$$H = (p_{02} - p_{01})/\rho \qquad (5)$$

Theoretical head comes from Euler relation:

$$H_t = c_{2u} \cdot u_2 - c_{1u} \cdot u_1 \qquad (6)$$

Finally, the impeller hydraulic efficiency is obtained as ratio of the effective and theoretical head:

$$\eta = H / H_t \qquad (7)$$

COMPUTATIONAL RESULTS

Comparison of Impeller Head and Efficiency

Computational results are outlined in Table 1. Hydraulic efficiency of the cantilever impeller is higher by 2 percent units versus the impeller with through-pass shaft. This agrees with experimental data, where the model pump efficiency is higher by 2 percent units with the cantilever impeller. The last result ensures that computations bring at least a reliable comparative result although the absolute values of impeller hydraulic efficiency looks underestimated.

Table 1. Comparison of Impeller Head and Efficiency Computational Results.

Parameter	Impeller # 1	Impeller # 2
H, m	73.3	77.6
H_t, m	78.4	81.3
η, %	93	95

Centrifugal Impellers Cavitational Quality

For analysis of cavitational quality of two centrifugal impellers the computational grid is changed in such a way that it provides an additional refinement of grid in the inlet section of the impeller and gives a denser grid without increase of required computer resources and processor time. Computation is made by unsteady method for seven full turns of impeller. That gives an appropriate convergence—performance parameters of impeller are close to previously obtained values.

The main parameter taken for this analysis is naturally the static pressure. In this way it gives a direct view of pressure distribution at the impeller inlet and on blade surfaces.

At the impeller inlet a few equidistant plane sections numbered from 1 to 5 are selected. The distance between sections is 3 mm. Plane 3 approximately corresponds to blade inlet edges at the cascade periphery.

Comparative analysis of pressure distribution in control planes and pressure plots on periphery of plane 2 shows that there is an essentially bigger step-wise nonuniformity of pressure in the impeller #1 than in impeller #2 (Figure 18 and 19). In plane 2 a local zone of negative pressure can be seen (the circle plot scale is from 0 to 90,000 Pa), indicating conditions for the cavitation inception.

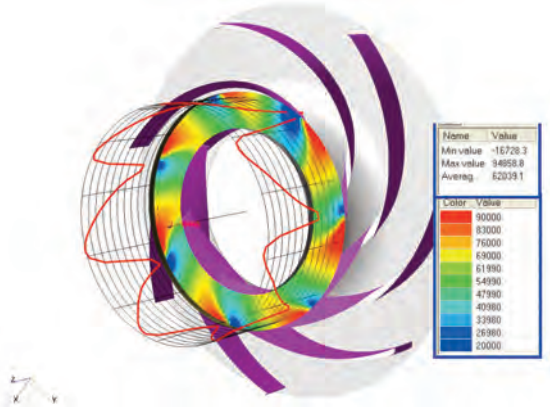

Figure 18. Static Pressure, Pa; Plane 2, Impeller #1.

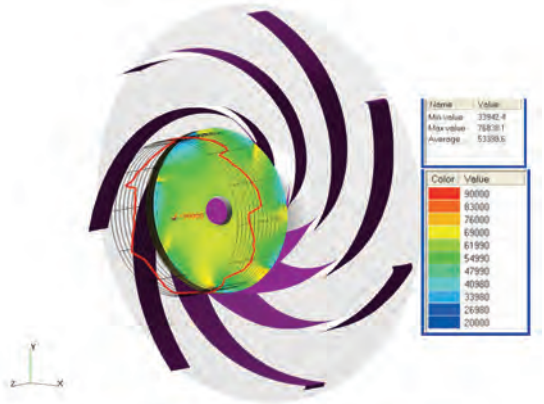

Figure 19. Static Pressure, Pa; Plane 2, Impeller #2.

In this computational method, appearance of cavitational bubbles and cavities is not simulated, that is why the computed pressure can be negative. The negative pressure is not corrected in a computational process. The question regarding such an artificial correction is disputable. Such a correction (example, pressure limit by a saturation level) in the model of incompressible fluid can distort the velocity field and complicate the computational data analysis. Since the negative pressure values appear in local zones, this does not complicate the analysis and indicates zones of cavitation inception. Inlet pressure field of impeller #2 is more uniform. Negative zones appear only in plane 3, i.e., at the periphery of the blade inlet edges.

Pressure distribution on blade surfaces also presents a lower pressure level on the suction side of the blade inlet part of impeller #2 (Figure 20, Figure 21). Such a pressure character corresponds with the flow velocity level. In Figure 22 and Figure 23 are color maps of the relative velocity module in control plane 3. It can be seen that velocity level in impeller #1 is considerably higher.

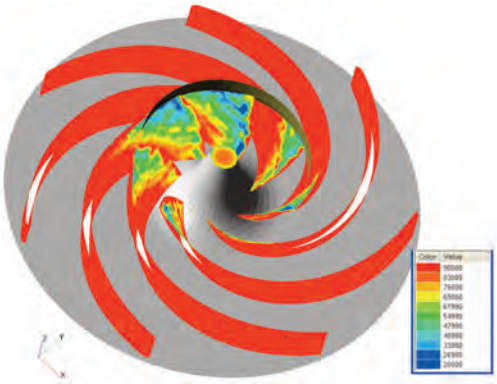

Figure 20. Pressure on Blade Surfaces, Pa; Impeller #2.

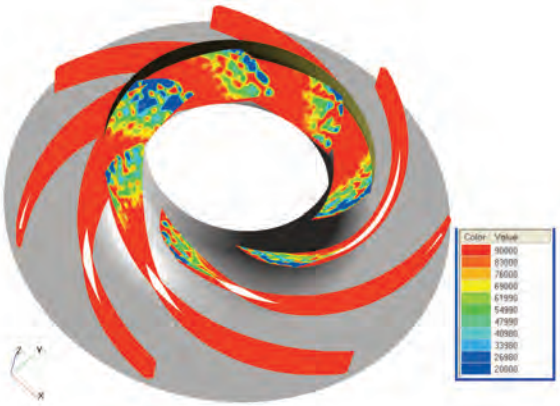

Figure 21. Pressure on Blade Surfaces, Pa; Impeller #1.

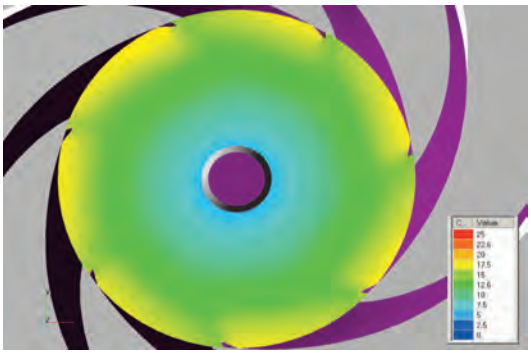

Figure 22. Relative Velocity Module in Plane 3, m/s; Impeller #2.

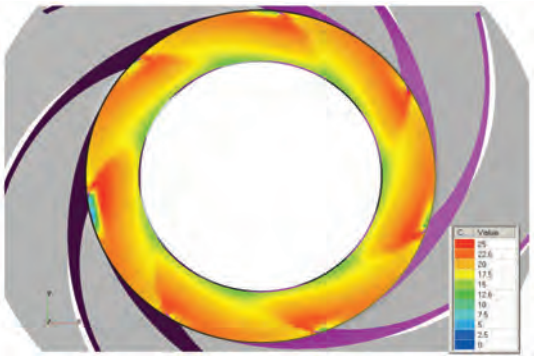

Figure 23. Relative Velocity Module in Plane 3, m/s; Impeller #1.

This reflects on the pressure distribution in the core flow. In Figure 24 for impeller #1 local zones are presented in the core flow where pressure level is equal or lower than 20,000 Pa. In impeller #2 such zones are practically absent.

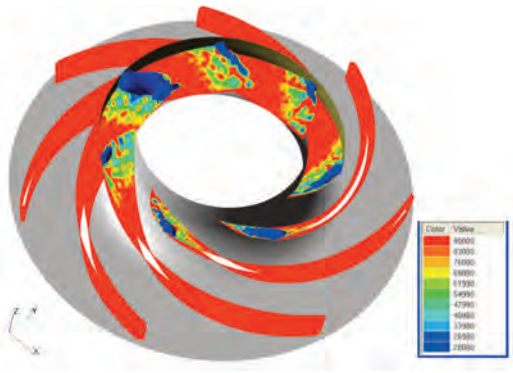

Figure 24. Pressure on Blade Surfaces and Pressure Zones Limited by 20,000 Pa; Impeller #1.

Analysis of pressure change in direction normal to the blade surface in the zone of minimal pressure shows that the pressure gradient by an order of magnitude on blade surfaces of impeller #1 is 10000 Pa/mm while in impeller #2 this parameter produces 10 Pa/mm.

The results obtained show that the pressure field at the centrifugal impeller inlet is unsteady with pressure pulsations of blade passing frequency and its harmonics. Under presence of inlet nonuniformity of flow, caused by the pump inlet device, it can generate oscillations of combined frequencies:

$$f_k = (z_1 \pm r) \cdot k \cdot n / 60 \qquad \textbf{(8)}$$

where:

z_1 = Number of impeller blades
r = Circular symmetry order of the inlet non-uniformity
k = Integer

Using this method (Knyazev, et al., 2007), computations of cavitating bubbles' evolution under nonuniform pressure field were

completed that show that the near-surface blade non-uniform pressure distribution causes an essential influence on cavitation erosion.

The following assumptions are taken:

- Water saturation pressure is p_s = 10 kPa, and
- Initial pressure in the cavitation nucleus bud is p_a = 10 kPa.

Cavitation on the blade surface is possible in a flow region, where pressure on the surface $p_w < p_{in}$, p_{in} being the pressure of cavitation inception. In the calculation it is assumed p_{in} = 14.9 kPa.

During its evolution the cavitating bubble transits downstream in the region of a higher pressure. Besides, the growing bubble penetrates into the flow core, where the pressure differs from the one at the wall. For evaluation of pressure gradients, the characteristic distance from the wall is taken as 1 mm. In case of a negative normal pressure gradient (i.e., the pressure reduces when moving away from the wall), there are created favorable conditions for the bubble separation with the subsequent collapse in the flow core. This case is of no interest in the study of cavitation erosion and it will not be under consideration. Due to the same reason the zero normal pressure gradient is out of consideration. In the last case cavitating bubbles can grow up to a very large size (more than 1 mm), separate from the wall and further collapse downstream in the region of higher pressure. Cases with positive normal pressure gradient are calculated.

Comparative analysis of pressure distribution obtained by 3D CFD computations shows that in impeller #1 pressure nonuniformity is considerably higher than in impeller #2. Pressure distribution on the blade surface also reveals lower pressure level on the suction side of blade inlet zones of impeller #1.

Supposed flow region with cavitation development is characterized by a pressure level in flow as ≈ 20 kPa and less. Computations are completed for three points with initial pressure in the flow core p_f = (20, 10, 5) kPa.

For each computational point there is a set of wall pressure values p_w, where $p_w < p_f$. Example, in the computational point p_f = 20 kPa cavitation is possible if p_w < 14.9 kPa, i.e., the pressure gradient on the distance 1mm must be less than 5.1 kPa.

Under increase of positive pressure gradient on one side the pressure wall value decreases and creates favorable conditions for cavitation inception, while from the other side it increases pressure unevenness on the bubble contour and its deformation in the evolution process, which gets a decrease of surface curvature on the bubble pole with development of the axial jet during bubble collapse. The final bubble shape presents a tear. It is important to note that in this case the vapor-gas phase does not disappear fully. Figure 25 and Figure 26 present the above mentioned evolution, the computational point—flow pressure p_f = 5 kPa, wall pressure p_w 2 kPa.

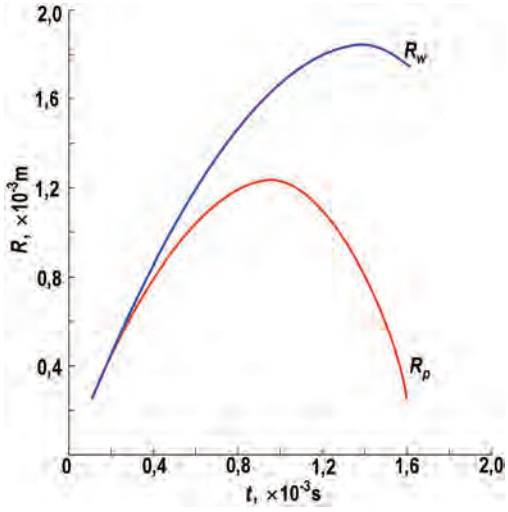

Figure 25. Change in Time of the Radius-Vector of the Cavitating Bubble Surface Points at the Pole Rp and on the Wall Rw.

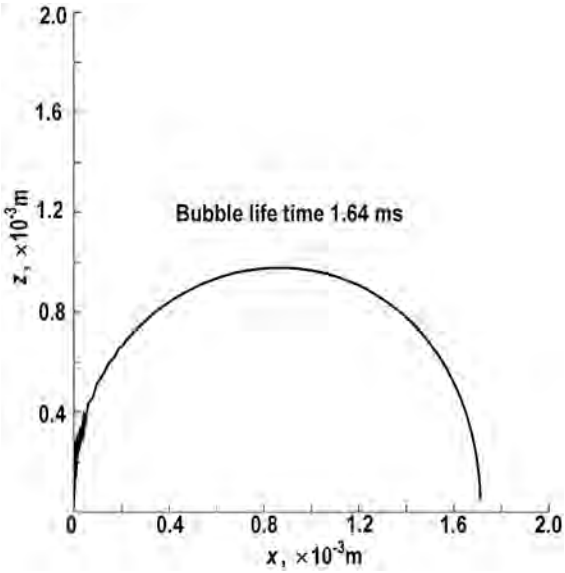

Figure 26. Shape of Bubble in the Moment of Collapse (Right-Hand Side Outlined).

Figure 25 presents a time change of the radius-vector of the cavitating bubble surface points on pole R_p and wall R_w. It can be seen that after one millisecond on the pole the bubble growth stops while on the wall the growth continues. The bubble lifetime is 1.64 milliseconds. In Figure 26 the bubble shape is presented in the collapse moment. The right half of the meridian bubble section is outlined. X-ax gives wall coordinates and Z-ax gives coordinates along the normal wall. It appears that the biggest deformation takes place in the pole region. Along the bubble axis a liquid jet forms. In Figure 27 is shown the pressure impulse on the bubble contour during its collapse, where J is the computational node number from the pole. The pressure pulse during jet braking produces 36 Mpa.

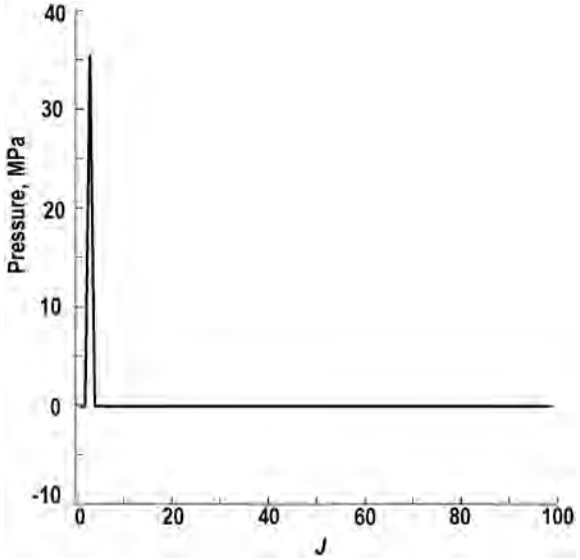

Figure 27. Pressure Distribution along the Contour in the Moment of Bubble Collapse, J - Number of Calculated Node from the Pole.

In Figure 28 computational results are presented for the wall stress during the bubble collapse in dependence of normal wall pressure gradient for three flow core pressure values p_f = (20, 10, 5) kPa. For all computational points it is found that a strong dependence of the wall stress level from both wall normal pressure gradient and the flow core pressure.

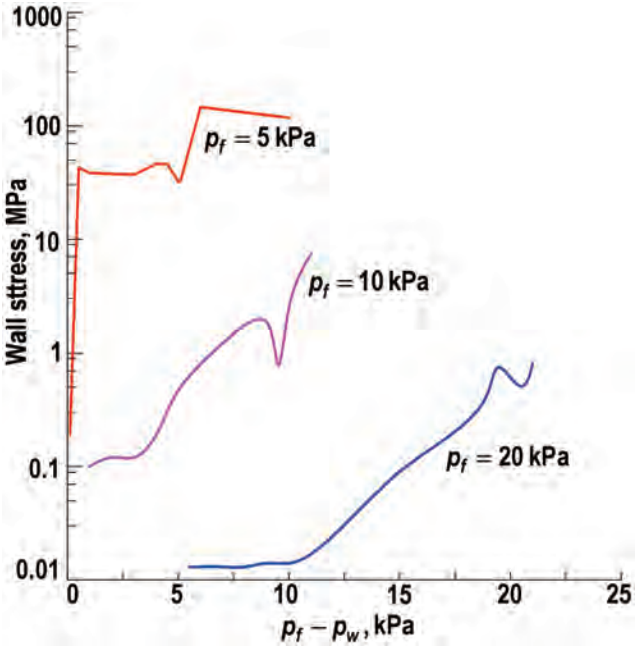

Figure 28. Wall Stresses under Cavitating Bubble Collapse in Dependence on Wall Pressure Normal Gradient.

In 3D CFD modeling of impeller #2 there is no considerable blade surface pressure gradient found. On cavitation erosion evaluation, one does not wait for cavitation erosion of the surface and this agrees with experimental data analysis. With a positive pressure gradient more than 5 kPa (in bounds of one mm layer) in the zone of possible cavitation development, during the bubble collapse stress makes up to 40 MPa (5800 psi), that appears to be enough for erosion damage of the varnish coating of impeller #1.

CONCLUSIONS

New computational procedure for evaluation of potential cavitation erosion damage is proposed and validated with experimental results for two impeller designs. The procedure comprises 3D unsteady flow analysis and calculation cavitating bubbles' statistical ensemble behavior in the nonuniform pressure and velocity field. It is proved that wall pressure normal gradient plays a crucial role in the level of wall stresses due to cavitating bubble collapse.

NOMENCLATURE

$C = n\sqrt{Q}/(\Delta h/10)^{3/4}$	= Suction specific speed (rpm, m^3/s, m)
D, d	= Diameter, m
$D_Q = \sqrt[3]{Q/n}$	= Reduced diameter
$\bar{d} = d/D$	= Hub relation
H	= Head, m
H_t	= Theoretic head, m
Δh	= NPSH, m
$K_0 = D_0/D_Q$	= Reduced eye diameter coefficient
$N = gQH/\eta$	= Power consumption, W
n	= Shaft speed, rpm
$n_s = 3.65n\sqrt{Q}/H^{3/4}$	= Specific speed (rpm, m^3/s, m)
p	= Pressure, Pa
p_v	= Saturated vapor pressure, Pa
Q	= Volumetric flow rate, m^3/s
η	= Efficiency
λ	= Cavitation coefficient
L_a	= Pump housing vibration level, dB
L_{cav}	= Cavity length, mm

Indices

1	= Impeller eye
2	= Impeller outlet
I, III	= First, third critical cavitation mode
3%	= Three percent head drop (e.g., refer to Figure 9)
¯	= Normalized value
BEP	= Best efficiency point

REFERENCES

Gopalakrishnan, S., 1985, "Modern Cavitation Criteria for Centrifugal Pumps," *Proceedings of the Second International Pump Symposium*, Turbomachinery Laboratory, Texas A&M University, College Station, Texas, pp. 3-10.

Gülich, J. F., 1992, "Diagnosis of Cavitation in Centrifugal Pumps," *World Pumps, 308*, pp. 15-20.

Gülich, J. F., 1997, "Moglichkeiten und Grenzen der Vorausberechnung von Kavitationsschaden in Kreiselpumpen," *Forsch Ingenieurwes, 63*, (1-2), pp. 27-39.

Gülich, J. F. and Pace, S., 1986, "Quantitative Prediction of Cavitation Erosion in Centrifugal Pumps," Proceedings of the 13th IAHR Symposium, September, Montreal, Canada, pp. 1-17.

Knyazev, V. A., Soldatov, V. A., and Rohatgi, U. S., 2007, "Evolution of a Cavitating Bubble in a Nonuniform Pressure Field," Proceedings of FEDSM2007 5th Joint ASME/JSME Fluids Engineering Conference, July 30-August 2, San Diego, California.

Panaiotti, S. S., Rohatgi, U. S., Timushev, S. F., Soldatov, V.A., and Chumachenko, B. N., 2007, "CFD Study of Prospective 1st Stage Centrifugal Impeller Design," CD Proceedings of FEDSM2007 5th Joint ASME/JSME Fluids Engineering Conference, July 30-August 2, San Diego, California.

Sloteman, D. P., Robertson, D. A., and Margolin, L., 2004, "Demonstration of Cavitation Life Extension for Suction-Stage Impellers in High Energy Pumps," *Proceedings of the Twenty-First International Pump Users Symposium*, Turbomachinery Laboratory, Texas A&M University, College Station, Texas, pp. 103-115.

Visser, F. C., Backx, J. J. M., Geerts, J., Cugal, M., and Torres, M. M., 1998, "Pump Impeller Lifetime Improvement Through Visual Study of Leading-edge Cavitation," *Proceedings of the Fifteenth International Pump Users Symposium*, Turbomachinery Laboratory, Texas A&M University, College Station, Texas, pp. 109-118.